Complex Degree of Mutual Polarization of Biotissue's Speckle-Images

Ye.G. Ushenko

Chernivtsi National University, 2 Kotsyubinsky St., 58012 Chernivtsi, Ukraine
ushenko-bio@itf.cv.ukrtel.net

Received 14.03.2005

Abstract

The article is directed to studies for the statistics of coordinate distributions of the complex degree of mutual polarization (CDMP) characterising biotissues' images. Diagnostic possibilities of the 2D distributions of the images' CDMP corresponding to physiologically normal and degeneratively-dystrophically changed biological tissues are analysed.

Key words: CDMP, biological tissues

PACS: 42.62.-b, 42.62.Be, 42.25.Lc, 42.25.Ja

1. Introduction

Polarization methods for researching the structure of biological tissue (BT) are traditionally based on the analysis of polarization degree $P(r)$ as a correlation function between the complex orthogonal components E_x and E_y of electromagnetic oscillations at some point (r) of the scattered radiation field.

Real object BT fields, including their images, manifest also spatial changes in both the polarization and the correlation characteristics [1-4]. A new methodological approach has been recently proposed for analysing these fields [5, 6]. It is based on generalization of the coherence matrix $\{\mathrm{K}(r,\tau)\}$ to the two-point (r_1,r_2) polarization coherence matrix

$$\{\Phi(r_1,r_2,\tau)\}:\{\mathrm{K}(r,\tau)\}\Rightarrow\{\Phi(r_1,r_2,\tau)\}, \quad (1)$$

$$\begin{Vmatrix} \langle E_x(r,\tau)E_x^*(r,\tau)\rangle & \langle E_x(r,\tau)E_y^*(r,\tau)\rangle \\ \langle E_x{}^*(r,\tau)E_y(r,\tau)\rangle & \langle E_y(r,\tau)E_y^*(r,\tau)\rangle \end{Vmatrix} \Rightarrow \begin{Vmatrix} \langle E_x(r_1,\tau)E_x^*(r_2,\tau)\rangle & \langle E_x(r_1,\tau)E_y^*(r_2,\tau)\rangle \\ \langle E_x{}^*(r_1,\tau)E_y(r_2,\tau)\rangle & \langle E_y(r_1,\tau)E_y^*(r_2,\tau)\rangle \end{Vmatrix}. \quad (2)$$

According to Eq. (2), the main parameter that determines a correlation interrelation between differently polarised points (r_1,r_2) of the object field with the intensities $I(r_1,\tau)$ and $I(r_2,\tau)$ is a complex degree of mutual polarization (CDMP) $V^2(r_1,r_2,\tau)$ [6]. The latter is written in the following form

$$V^2(r_1,r_2,\tau)=4\frac{\nu_1^2+\nu_2^2+\nu_3^2}{I(r_1,\tau)I(r_2,\tau)}, \quad (3)$$

where the coefficients ν_i are defined by the relations

$$\nu_1=\frac{\langle E_x(r_1,\tau)E_x^*(r_2,\tau)\rangle-\langle E_y(r_1,\tau)E_y^*(r_2,\tau)\rangle}{2},$$
$$\nu_2=\frac{\langle E_x(r_1,\tau)E_y^*(r_2,\tau)\rangle-\langle E_y(r_1,\tau)E_x^*(r_2,\tau)\rangle}{2}, \quad (4)$$
$$\nu_3=i\frac{\langle E_x(r_1,\tau)E_y^*(r_2,\tau)\rangle-\langle E_y(r_1,\tau)E_x^*(r_2,\tau)\rangle}{2}.$$

They have a meaning of numerical differences between the interference pattern visibilities at the points r_1 and r_2, which are measured through differently oriented polarization filter (ν_1 corresponds to the angles 0^0 and 90^0 of the transmission axis of analyser, ν_2 to 45^0 and

135^0 and ν_3 to the right- and left-handed circular polarizations).

Up to date, not too many publications has been known, dedicated to direct measurements of the CDMP for the statistical fields of the scattered laser radiation (see [7-10]). Nonetheless, the approach seems to be urgent for the biomedical optics, concerned with a processing of coherent polarization-inhomogeneous BT images [11] obtained with the techniques of optical coherent tomography.

This paper deals with elaboration of the technique for measuring 2D CDMP distributions for the BT speckle-images ($2D[V^2]$), in order to find interrelations between the statistical moments of the CDMP of first to fourth orders and the peculiarities of birefringent architectonic nets of the types of fibrillar protein (collagen and myosin) nets and the ensembles of "island" birefringent collagen formations.

2. Theoretical modelling

Let us consider two differently polarised laser oscillations at the points r_1 and r_2 of the BT image,

$$\begin{cases} E_x(r_1)+E_y(r_1)\exp(-i\delta_1(r_1)), \\ E_x(r_2)+E_y(r_2)\exp(-i\delta_2(r_2)). \end{cases} \quad (5)$$

Here $\delta_1(r_1)$ and $\delta_2(r_2)$ are the phase shifts between the orthogonal components of the complex amplitudes E_x and E_y at the points r_1 and r_2.

Under the conditions of completely correlated laser BT image, the generalised coherence matrix (see Eq. (2)) becomes

$$\{\Phi(r_1,r_2)\} = \left\| \begin{matrix} E_x(r_1)E_x^*(r_2) & E_x(r_1)E_y^*(r_2) \\ E_x{}^*(r_1)E_y(r_2) & E_y(r_1)E_y^*(r_2) \end{matrix} \right\|. \quad (6)$$

Taking Eqs. (5) into account, one can rewrite the operator in Eq. (6) as

$$\{\Phi(r_1,r_2)\} = \left\| \begin{matrix} E_x(r_1)E_x(r_2) & E_x(r_1)E_y(r_2)\exp(i\delta(r_2)) \\ E_y(r_1)E_x(r_2)\exp(i\delta(r_1)) & E_y(r_1)E_y(r_2) \end{matrix} \right\|. \quad (7)$$

Using Eq. (7) and accounting for Eq. (3) and Eq. (4), one can show that the CDMP for the two image points under consideration is described with the relation

$$V^2(r_1,r_2) = \frac{\left(E_x(r_1)E_x(r_2)-E_y(r_1)E_y(r_2)\right)^2 + 4E_x(r_1)E_x(r_2)E_y(r_1)E_y(r_2)\exp\left(i(\delta_2(r_2)-\delta_1(r_1))\right)}{\left(E_x^2(r_1)+E_y^2(r_1)\right)\left(E_x^2(r_2)+E_y^2(r_2)\right)}. \quad (8)$$

The values of the local phase shifts $\delta_1(r_1)$ and $\delta_2(r_2)$ are concerned with the parameters $\alpha\begin{pmatrix} r_1,...r_m \\ ..... \\ r_n,...r_m \end{pmatrix}$ and $\beta\begin{pmatrix} r_1,...r_m \\ ..... \\ r_n,...r_m \end{pmatrix}$ of the polarization map of BT speckle-image through the following relations [1]:

$$\delta(r_1) = \arctan\left[\frac{\tan 2\beta(r_1)}{\tan\alpha(r_1)}\right], \qquad \delta(r_2) = \arctan\left[\frac{\tan 2\beta(r_2)}{\tan\alpha(r_2)}\right]. \quad (9)$$

The analysis of Eq. (5) – (9) testifies that the range of changes for the CDMP $V^2(r_1,r_2)$ is wide enough, depending upon different polarization states of the light oscillations $E(r_1)$ and $E(r_2)$ at the points r_1 and r_2. Its limiting values are 0.0 for the orthogonal states and 1.0 for the collinear states. The possible values of the CDMP may be illustrated by the Table 1.

The values of $\alpha(r_1,...r_m), \beta(r_1,...r_m)$ and $E_x(r_1,...r_m), E_y(r_1,...r_m)$ at every point of the BT image are linked with the orientational ($\rho(r_1,...r_m)$) and the phase ($\delta(r_1,..r_m)$) parameters of its architectonics:

$$\alpha(r_i)=0.5\arctan\left[\frac{\sin 4\rho(r_i)\sin^2 0.5\delta(r_i)}{\cos^2 2\rho(r_i)+\sin^2 2\rho(r_i)\cos\delta(r_i)}\right],$$
$$\beta(r_i)=0.5\arcsin\left[\frac{\tan 2\rho(r_i)}{\sin\delta(r_i)}\right], \tag{11}$$

$$E_x(r_i)=\left\{I_0\left[\sin^2\alpha(r_i)+\cos^2\alpha(r_i)\tan^2\beta(r_i)\right]\right\}^{1/2},$$
$$E_y(r_i)=\left\{I_0\left[\cos^2\alpha(r_i)+\sin^2\alpha(r_i)\tan^2\beta(r_i)\right]\right\}^{1/2}. \tag{12}$$

Thus, the CDMP of the BT speckle-image appears to be a parameter sensitive to any changes in the orientation and phase architectonics. Moreover, it may be obtained with direct experimental measurements:

$$V^2(r_{n+k},r_n)=\frac{\left(\left(I^{(0)}(r_{n+k})I^{(0)}(r_n)\right)^{\frac{1}{2}}-\left(I^{(90)}(r_{n+k})I^{(90)}(r_n)\right)^{\frac{1}{2}}\right)^2}{I(r_{n+k})I(r_n)}+$$
$$+\frac{4\left(I^{(0)}(r_{n+k})I^{(90)}(r_{n+k})I^{(0)}(r_n)I^{(90)}(r_n)\right)^{\frac{1}{2}}\cos(\delta_{n+k}(r_{n+k})-\delta_n(r_n))}{I(r_{n+k})I(r_n)}. \tag{13}$$

Here $I^{(0)}(r_i)$ and $I^{(90)}(r_i)$ are the arrays of the BT image intensities measured for the orientations of transmission axis of analyser that correspond to the angles $\Theta=0^0$ and $\Theta=90^0$.

3. Analysis and discussion of experimental data

Histological sections of myocardium (MT), kidney (KT) and spleen (ST) tissues were used as investigation objects. The experimental part contains the data $2D[V^2(\Delta r_i)]$ for the BT speckle-images obtained with discretization interval $\Delta r_i=1$ CCD pixel (see Fig. 1a – Fig. 3a), as well as the probability distributions $Q[V^2(\Delta r_i)]$ and the corresponding statistical moments of the first to fourth orders (see Fig. 1b to Fig. 3b, and Table 2).

The analysis of the data derived by us reveals the follows.

(i) The distributions $2D[V^2(\Delta r_i)]$ of the speckle-images differ essentially for different types of the BT.

(ii) $2D[V^2(\Delta r_i)]$ of the MT images

Table 1. The possible values of the CDMP

$E(r_1)$	$E(r_2)$	$V^2(r_1,r_2)$
$E_x(r_1)$; $E_x(r_1)+E_y(r_1)\exp(i\delta)$	$E_x(r_2)$; $E_x(r_2)+E_y(r_2)\exp(i\delta)$	1
$E_x(r_1)$	$E_x(r_2)+E_y(r_2)$	$\frac{E_x^2(r_2)}{E_x^2(r_2)+E_y^2(r_2)}$
$E_x(r_1)$	$E_x(r_2)+iE_y(r_2)$	0.5
$E_x(r_1)$; $E_x(r_1)+E_y(r_1)\exp(i\delta)$	$E_y(r_2)$; $E_x(r_2)-E_y(r_2)\exp(i\delta)$	0

Table 2. Statistics of CDMP for the BT speckle-images.

MT (37 samples)		KT (34 samples)		ST (35 samples)	
M_{V^2}	0.18	M_{V^2}	0.24	M_{V^2}	0.03
σ_{V^2}	0.11	σ_{V^2}	0.18	σ_{V^2}	0.02
A_{V^2}	67.4	A_{V^2}	259.3	A_{V^2}	17.4
E_{V^2}	324.2	E_{V^2}	874.9	E_{V^2}	26.9

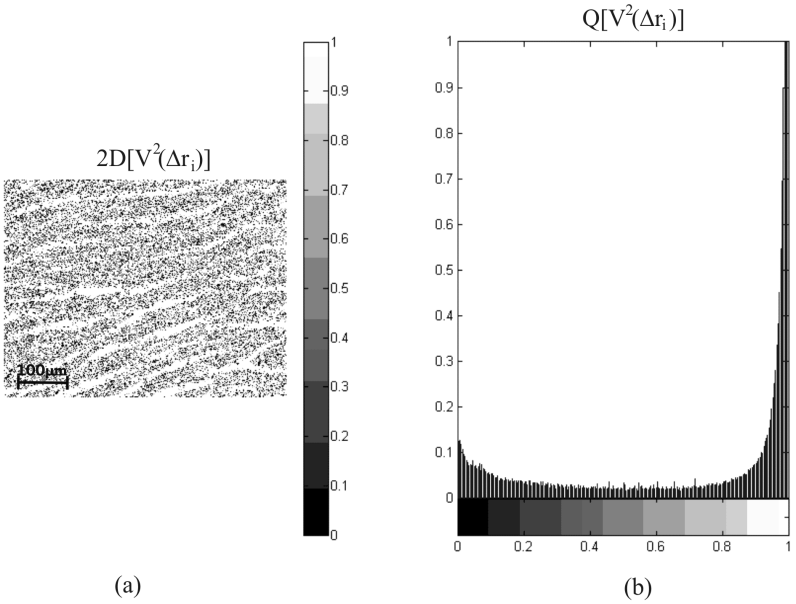

Fig. 1. Coordinate (a) and statistical (b) structures of the CDMP for the MT speckle-image.

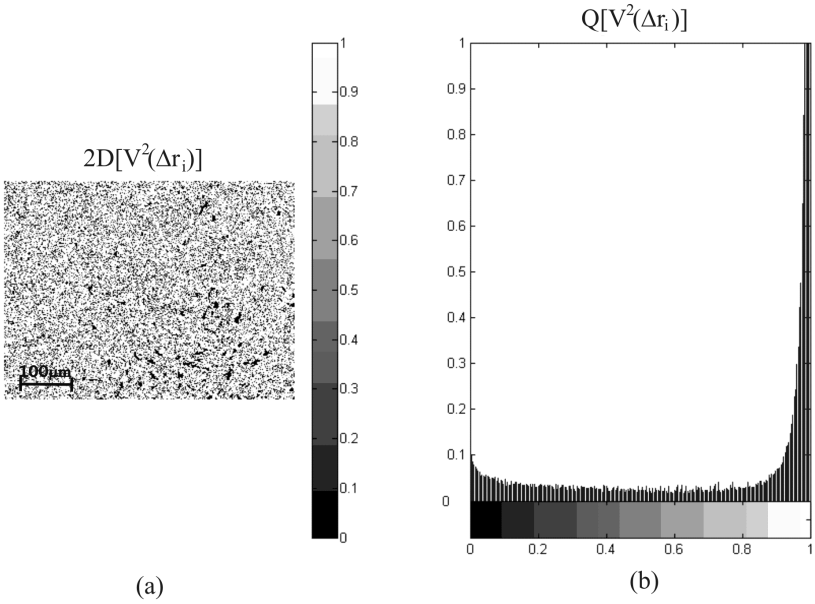

Fig. 2. Polarization-correlation structure of the KT speckle-image.

obtained for $\Delta r_i = 1$ are formed mainly by large-scale ($25 \div 100$ μm) regions with the most correlated polarization states ($V^2(\Delta r_i) \to 1$). Statistically this points out to extremum on the basic

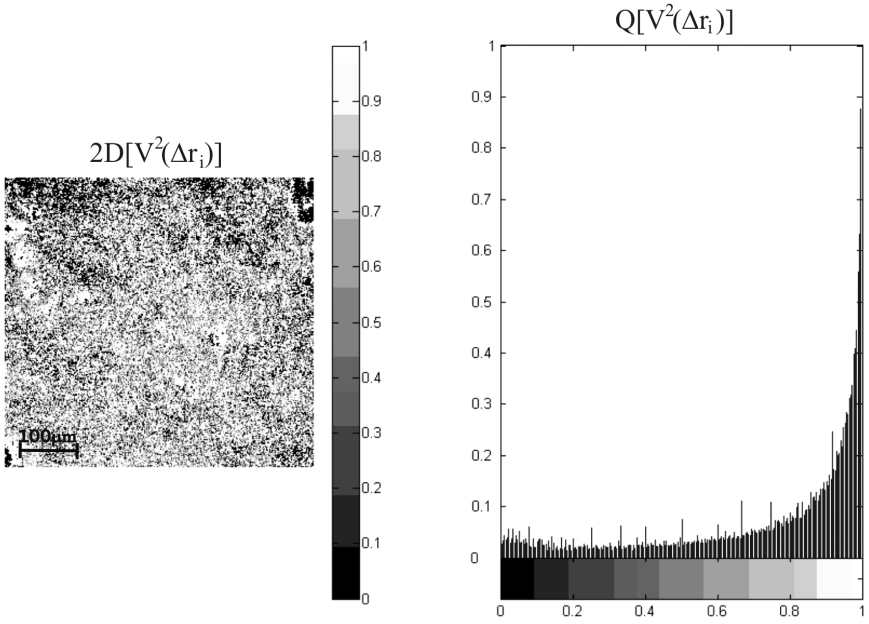

Fig. 3. Coordinate (a) and statistical (b) structures of the CDMP for the ST speckle-image

histogram ($Q[V^2(\Delta r_i)]$) (see Fig. 1b). Along with this fact, $2D[V^2(\Delta r_i)]$ have regions where the CDMP changes in a wide range ($0 \le V^2(\Delta r_i) \le 1$). This produces the corresponding additional extrema on the histogram $Q[V^2(\Delta r_i)]$.

(iii) Except for the areas of maximum polarization correlation, differently scaled ($10 \div 30$ μm) regions, where the CDMP changes in a wide range ($0 \le V^2(\Delta r_i) \le 1$) (see Fig. 2a), form the $2D[V^2(\Delta r_i)]$ distribution for the coherent images of the MT. In case of laser KT images (Fig. 2b), the histograms $Q[V^2(\Delta r_i)]$ also manifest a set of considerably equiprobable extrema for actually a whole range of CDMP values.

(iv) The correlation structure of the polarization states of the speckle-images points to essential prevalence of their polarization-homogeneous component. The $2D[V^2(\Delta r_i)]$ distributions (see Fig. 3a) may be considered as a set of regions with the extreme CDMP value $V^2(\Delta r_i) \to 1$. By its structure, the histogram in Fig. 3b is close to δ function of the form

$$Q[V^2(\Delta r_i)] = \begin{cases} 1[V^2(\Delta r_i) = 1], \\ \to 0[V^2(\Delta r_i) \ne 1]. \end{cases}$$

The statistical moments of $Q[V^2(\Delta r_i)]$ of the first to fourth orders for the different BT types are gathered in Table 2.

Notice that the statistical CDMP moments mentioned above have been calculated, using the relationships

$$\begin{aligned} M_{V^2} &= \frac{1}{N}\sum_{i=1}^{N}\left|V^2(\Delta r_i)\right|, \\ \sigma_{V^2} &= \sqrt{\frac{1}{N}\sum_{i=1}^{N}(V^2(\Delta r_i))^2}, \\ A_{V^2} &= \frac{1}{\sigma_{V^2}^3}\frac{1}{N}\sum_{i=1}^{N}(V^2(\Delta r_i))^3, \\ E_{V^2} &= \frac{1}{\sigma_{V^2}^2}\frac{1}{N}\sum_{i=1}^{N}(V^2(\Delta r_i))^4, \end{aligned} \tag{14}$$

where $N = m \times n$ denotes the overall amount of the CDMP values.

The $2D[V^2(\Delta r_i)]$ structure for the BT speckle-images under consideration is closely concerned with different morphological structures of their architectonics. According to Eqs. (8), (11) and (12), the packaging order of

myosin fibrils in the MT, peculiar for considerably large geometrical domains, stipulates a high degree of correlation identity ($V^2(\Delta r_i)\to 1$) for the polarization states of the corresponding speckle-image points. Transition to the other domains (the parts with different orientational architectonic structures) is accompanied with decreasing CDMP for the given image parts. However, the degree of mutual polarization of the MT speckle-image points extremely increases again within each domain (see Fig. 1a).

There are more dynamic $V^2(\Delta r_i)$ changes that occur for the image points of different parts of architectonic net in the case of 2D CDMP distribution for the speckle-images of collagens oriented chaotically. Besides of the main maximum, the statistical distributions $Q[V^2(\Delta r_i)]$ are then formed by considerably equi-probable extrema (Fig. 2b), which are caused by a variety of orientational KT architectonic structures and a decrease of their self-similar geometrical sizes (see Fig. 2a).

The $2D[V^2(\Delta r_i)]$ structure for the ST speckle-images represents a highly correlated interrelation between the polarization states at different points, with a completely polarization-homogeneous character of the speckle-image (see Fig. 3a and 3b).

A comparative analysis of statistical moments of the parameter $V^2(\Delta r_i)$ of the first to fourth orders evidences that the following relations hold true:

$$\begin{aligned} &M_{V^2}(MT)\ge M_{V^2}(KT)\ge M_{V^2}(ST),\\ &\sigma_{V^2}(MT)\ge \sigma_{V^2}(KT)\ge \sigma_{V^2}(ST),\\ &A_{V^2}(MT)\ge A_{V^2}(KT)\ge A_{V^2}(ST),\\ &E_{V^2}(MT)\ge E_{V^2}(KT)\ge E_{V^2}(ST). \end{aligned} \qquad (15)$$

This analysis (see also Eqs. (15)) finds out a large sensitivity (the magnitude being varied by 2–5 times) of the statistical moments of the third and fourth orders to the peculiarities of orientational structure of architectonic nets, when compare with the analogous parameters of polarization maps $\alpha\begin{pmatrix} r_1,\dots r_m \\ \dots\dots \\ r_n,\dots r_m \end{pmatrix}$ and $\beta\begin{pmatrix} r_1,\dots r_m \\ \dots\dots \\ r_n,\dots r_m \end{pmatrix}$ of the BT speckle-images. That is why investigations of the possibilities of polarization-correlation analysis for the BT speckle-images, with the aim of diagnostics of their physiological state connected with the changes in architectonic net structure, seem to be topical.

4. Polarization-correlation structure of speckle-images of the birefringent BT nets and diagnostics of their pathological changes

In this part of our studies we search for interconnections between the polarization-correlation structure of the BT speckle-images and the optical and geometrical parameters of their physiologically normal and pathologically changed birefringent architectonic nets.

As the objects under test, we have used "optically thin" (the extinction coefficient $\tau\le 0.1$) histological BT sections of the following types: (i) physiologically normal (Fig. 4a) and dystrophically changed (Fig. 4b) myocardium muscle tissue (MT), and (ii) physiologically normal (Fig. 4c) tissue of the cannon bone and the bone tissue (BnT) affected with osteoporosis (Fig. 4d).

Morphological structure of the architectonics of such the BT is different. The MT is formed by quasi-ordered myosin fibrils and the fibres that form bundles (Fig. 4b), with the birefringence of their substance being equal to $\Delta n\approx 1.5\times 10^{-3}$ [12]. The BnT architectonics is featured by the oriented collagen fibres, which are mineralised by hydroxylapatite crystals ($\Delta n\approx 1.1\times 10^{-1}$, see Fig. 4d).

Early (pre-clinical) degenerative dystrophic changes in these tissues reveal themselves morphologically through various "scenarios". While the birefringence level remains unchanged, the myosin fibrils and fibres disorder within mono-

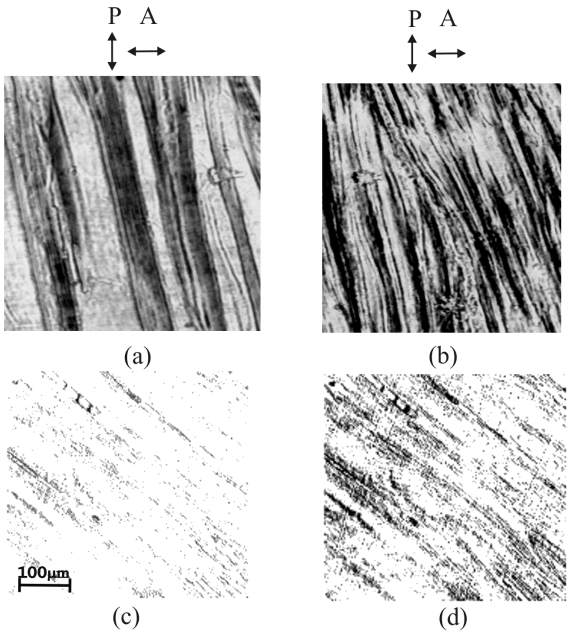

Fig. 4. Coherent images of architectonics for physiologically normal MT (a) and BnT (c) and dystrophically changed MT (b) and BnT (due to psoriasis) (d). The images are obtained for the crossed polarizer (P) and analyser (A). The arrows depict orientations of the transmission axes of polarizer (A) and analyser (B).

oriented MT bundles. The osteoporosis-affected MT exhibits a decrease in the concentration of hydroxylapatite crystals ($\Delta n \approx 10^{-2} \div 10^{-3}$), under the condition of unchanged orientational structure of the collagen net.

The coordinate CDMP distributions $2D[V^2(\Delta r_i)]$ for the coherent images of physiologically normal and degeneratively-dystrophically changed MT and BnT are illustrated in Fig. 5a, 6a and 5b, 6b, respectively. For the all types of BT, measurements of the intensities and polarization azimuths and ellipticities, necessary for calculations of $2D[V^2(\Delta r_i)]$, have been performed with the discretization parameter $\Delta r_i = 1$. Fig. 5c, 5d and Fig.6c, 6d present the histograms of probability distributions of the CDMP ($2D[V^2(\Delta r_i)]$).

The analysis of the data obtained for the coordinate and statistical structures of 2D CDMP distributions for the BT speckle-images may be summarised in the following.

(i) The $2D[V^2(\Delta r_i)]$ distributions for physiologically normal BTs of both types are rather close in their structures. They are mainly formed by the areas with maximally correlated polarization states ($V^2(\Delta r_i) \to 1$, see Fig.5a and 6a). From the statistical viewpoint, this fact is evidenced by the principal extremum of the corresponding histograms $Q[V^2(\Delta r_i)]$ (see Fig. 5c and 6c). Besides, $2D[V^2(\Delta r_i)]$ of such the images contain a small amount of areas with intermediate CDMP values ($0 \le V^2(\Delta r_i) \le 1$), with the additional $Q[V^2(\Delta r_i)]$ extrema corresponding to them.

(ii) $2D[V^2(\Delta r_i)]$ for the coherent images of degeneratively-dystrophically changed BT samples are formed by the areas, for which the CDMP value changes in a wide enough range ($0 \le V^2(\Delta r_i) \le 1$, see Fig. 5b and 6b). The corresponding histograms $Q[V^2(\Delta r_i)]$ contain a set of equi-probable extrema that characterise the whole range of CDMP changes for the coherent images of both the MT (Fig. 5d) and BnT (Fig. 6d).

(iii) The dependences $Q[V^2(\Delta r_i)]$ provide unbiased characterization by means of using the statistic moments of CDMP of the first to fourth orders (see Table 3).

The investigated $2D[V^2(\Delta r_i)]$ structures for the speckle-images of physiologically normal and degeneratively-dystrophically changed BTs are closely connected with various morphological structures of their architectonics. According to Eqs. (8), the packing order of the myosin and collagen fibrils in physiologically normal MTs and BnTs within rather large geometric domains of their architectonic nets causes a high correlation similarity ($V^2(\Delta r_i) \to 1$) of the polarization corresponding to different points of their coherent images. However, the degree of mutual polarization of the BT image points extremely increases again within the domains themselves.

Table 3. Statistics of first to fourth orders for the CDMP of BT speckle-images.

MT (37 samples)			BnT (34 samples)		
	Normal	Dystrophically changed		Normal	Affected by osteoporosis
M_{V^2}	0.18	0.96	M_{V^2}	0.24	0.85
σ_{V^2}	0.11	0.67	σ_{V^2}	0.18	0.45
A_{V^2}	67.4	589.7	A_{V^2}	87.3	967.7
E_{V^2}	32.2	451.3	E_{V^2}	74.9	798.3

The contrary tendency is observed for the 2D CDMP distributions in the case of coherent images of physiologically changed samples representing both types of the BTs. Morphological degenerative-dystrophic changes of the MT are accompanied by disordering fibril package in the myosin bundles. From the standpoint of optics, such the process is similar to increase in the angular interval between the polarization azimuth α_0 of illuminating laser beam and the "highest speed" axis $\rho(r_1,...r_m)$ of optically anisotropic structures. Various polarization states $\alpha(r_1,...r_m)$ and $\beta(r_1,...r_m)$ of the laser oscillations would be formed at the corresponding points of the MT coherent image. Thus, the CDMP fluctuations would increase, while the corresponding statistic distributions $Q[V^2(\Delta r_i)]$ would transform into a set of rather equiprobable extrema (see Fig. 5d).

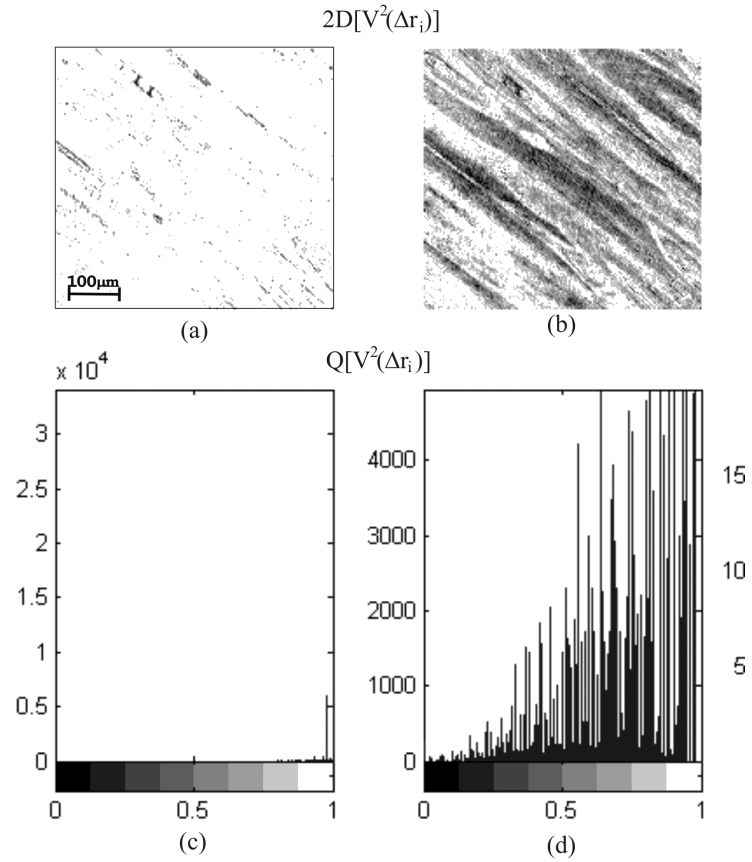

Fig. 5. Coordinate (a, b) and statistical (c, d) structures of the CDMP for the speckle-images of healthy (a, c) and pathologically changed by psoriasis (b, d) BnT.

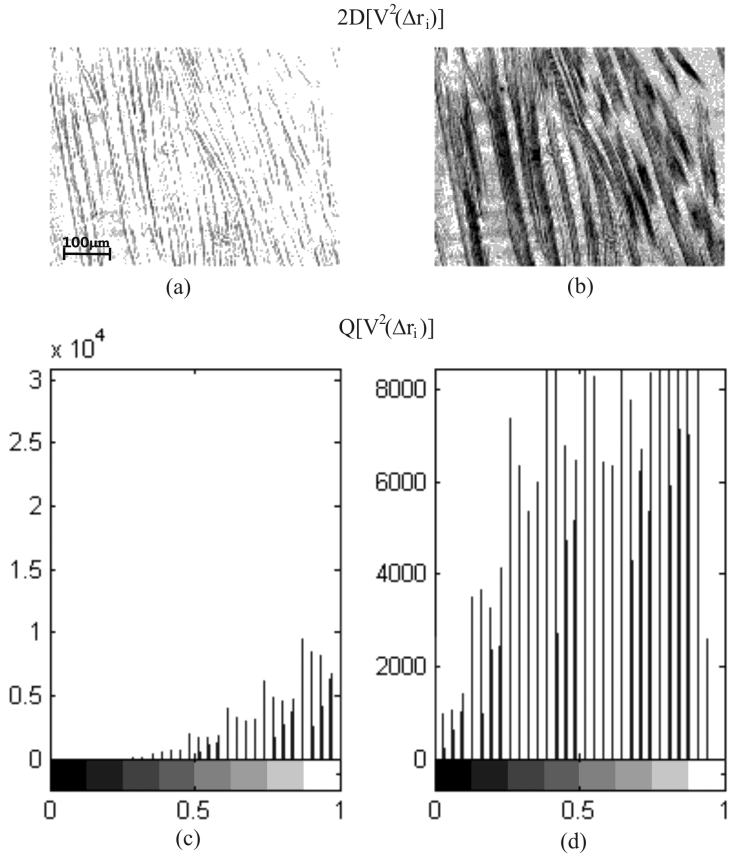

Fig. 6. Coordinate (a, b) and statistical (c, d) structures of the CDMP for the speckle-images of healthy (a, c) and pathologically changed by psoriasis (b, d) MT.

With regards to the optics, early manifestations of osteoporosis in the BnT could be represented by coordinate modulation of the phase shifts $\delta(r_1,...r_m)$ that the hydroxylapatite crystals introduce for the orthogonal components E_{0x} and E_{0y} of the illuminating laser radiation. These phenomena determine the coherent images. Under the conditions of unchanged orientational structure $\rho(r_1,...r_m)$ of the collagen fibres, it is just the modulation that mainly produces polarizationally inhomogeneous ($\alpha(r_1,...r_m)$ and $\beta(r_1,...r_m)$) parts in the BnT image. Then the $V^2(\Delta r_i)$ value associated with this process becomes statistical.

The comparative analysis of the statistic moments of $V^2(\Delta r_i)$ for the groups of physiologically normal ($M^*_{V^2}, \sigma^*_{V^2}, A^*_{V^2}$ and $E^*_{V^2}$) and pathologically changed ($M_{V^2}, \sigma_{V^2}, A_{V^2}$ and E_{V^2}) BTs of both structural types testifies the relations (see also Table 3)

$$M_{V^2} \geq M^*_{V^2}, \sigma_{V^2} \geq \sigma^*_{V^2}, A_{V^2} \geq A^*_{V^2}, E_{V^2} \geq E^*_{V^2}. \quad (16)$$

When the probability distributions of the form $Q[V^2(\Delta r_i)] = \begin{cases} 1\,[V^2(\Delta r_i) = 1] \\ \to 0\,[V^2(\Delta r_i) \neq 1] \end{cases}$ (see Fig. 6c and 6d) transform into a random-type ones ($0 \leq Q[V^2(\Delta r_i)] \leq 1$), the corresponding statistical moments of CDMP for the coherent images of degeneratively-dystrophically changed BT become larger. These differences are pronounced most of all (namely, the corresponding values differ by one order of magnitude) for the third and fourth statistical moments of the CDMP.

Conclusions

On the basis of polarization technique for measuring the 2D CDMP distributions for the BT

speckle-images, we have revealed the links between the statistical moments of the CDMP and the optical and geometrical structures of degeneratively-dystrophically changed architectonic nets of the MT and BnT. The information obtained for the polarization-correlation structure of the speckle-images that correspond to different morphological BT structures could be used in order to elaborate new methods for the analysis of their physiological states, when making use of the optical coherence tomography technique.

References

1. Sankaran V., Schonenberger K., Walsh J.T.Jr., Maitland D.J. Appl. Opt. **38** (1999) 4252.
2. Jarry G., Steimer E., Damaschini V., Epifanie M., Jurczak M., Kaiser R. Appl. Opt. **37** (1998) 7357.
3. Olar E.I., Ushenko A.G., Ushenko Yu.A. Laser Phys. **7** (2004) 1012.
4. Olar E.I., Ushenko A.G., Ushenko Yu.A. Laser Phys. **8** (2004) 1115.
5. Gori F. Opt. Lett. **23** (1998) 241.
6. Ellis J., Dogariu A. Opt. Lett. **29** (2004) 536.
7. Wolf E. Opt. Lett. **28** (2003) 5.
8. Mujat M., Dogariu A. Opt. Lett. **28** (2003) 2153.
9. Ellis J., Dogariu A., Ponomarenko S., Wolf E. Opt. Lett. **29** (2004) 1536.
10. Mujat M., Dogariu A., Agarwal G.S. Opt. Lett. **29** (2004) 1539.
11. Jiao S., Wang L.V. Opt. Lett. **27** (2002) 101.
12. Angelsky O.V., Ushenko A.G., Burkovets D.N., Ushenko Yu.A. J. Biomed. Opt. **10** (2005) 014010.